

Intra Vehicular Wireless Channel Measurements

Aniruddha Chandra¹, Aleš Prokeš¹, Jiří Blumenstein¹, Pavel Kukolev¹,
Josef Vychodil¹, Tomáš Mikulášek¹, Thomas Zemen²
and Christoph F. Mecklenbräuer³

¹Department of Radio Electronics, Brno University of Technology,
61600, Brno, Czech Republic

²AIT Austrian Institute of Technology GmbH, 1220, Vienna, Austria

³Institute of Telecommunications, Vienna University of Technology, 1040, Vienna, Austria
{chandra, prokes, blumenstein, mikulasek}@feec.vutbr.cz,
{xkukol01, xvycho05}@stud.feec.vutbr.cz, thomas.zemen@ait.ac.at,
christoph.mecklenbraeuer@tuwien.ac.at

Abstract. Intra vehicular communication is an emerging field of research due to its potential applications in safety of passengers, navigational and localization aids for driver, and multimedia infotainment. This chapter describes the wireless channel sounding activities performed inside a typical passenger car under the SoMoPro and the GACR projects. Three different channel sounding architectures are developed for the purpose, namely direct pulse based sounding, frequency domain sounding and pseudo noise sequence based time domain sounding. Experiments with different placements of transmitter and receiver antennas inside the car were performed for both the ultra-wide-band and millimeter wave band. Channel transfer functions and impulse responses extracted from all these measurement campaigns are utilized to construct several deterministic and statistical channel models. The models are useful for designing intra vehicular wireless links and for devising novel vehicular localization algorithms.

1 Background

In recent years there has been a growing demand for wireless personal area networks (WPANs) offering high data rates for short-range indoor communication applications. The manufacturers of vehicles, aircrafts, etc. have a great interest in replacing wired communication links by wireless one in order to save installation costs.

Intra vehicular wireless links are also pivotal for intra-vehicle sensor networks. Modern vehicles employ a large number of sensors to provide vital information such as temperature, wheel rotation speed, distances to nearby objects, etc., for the electronic control units. As the number of such sensors steadily increases, the physical wires between the electronic control unit and the sensors pose significant challenges in design because wires are expensive, wiring harness belong among the heaviest components in a vehicle and have a large impact on fuel consumption, and wires are also restrictive because there are a few locations in the vehicle where sensors cannot be deployed (steering wheel, tyres, and windshields).

Another aspect for intra vehicular wireless links to be considered is the possibility of object (device or people) localization. For example, pervasive electronic gadgets require

position specific instructions (e.g. hands-free profile for driver), the safety equipments such as smart air bags require knowledge of passenger occupancy, and personalized infotainment demands parallel location oriented multimedia streaming.

For such a wide range of intra vehicular wireless applications, the prospective candidates are, ultra-wide-band (UWB), millimeter wave (mmW), and infrared (IR) or optical band technologies. UWB technologies working in the 3.1 GHz to 10.6 GHz frequency band provides data rates up to a few Gbps for the short-range communication in WPANs. On the other hand, 60 GHz mmW band (55-65 GHz) offers low latency and high transmission capacity of up to 2 Gbps. Finally, IR communication has the advantages of utilizing unregulated and unlicensed electromagnetic spectrum, offers high quality data transmission, and is immune to electromagnetic interference.

1.1 GACR Project

The GACR project [1] is scheduled for four years (2013-2016) and is funded by the Czech Science Foundation. The title of the project is, 'Research into wireless channels for intra-vehicle communication and positioning'.

The main emphasis of the project is measurement and modeling of the intra-vehicle channel for WPAN application in the UWB, mmW, and optical bands and for object localization application in the UWB, and mmW bands. In addition, the existing mmW and UWB channel models derived for WPAN and sensor networks applications will be verified and compared with models created for optical bands.

The project includes six work packages as described below:

- WP 1:** Creation of the workplace for measurement of mmW, UWB, and optical signal propagation within the vehicle.
- WP 2:** Measurement of the intra-vehicle signal propagation for WPAN, sensor network and positioning applications.
- WP 3:** Analysis and modeling of mmW and UWB signal propagation for WPAN and sensor network application, verification and improvement of the existing channel models.
- WP 4:** Analysis and modeling of mmW and UWB signal propagation within the vehicle for the localization purposes.
- WP 5:** Analysis and modeling of the IR propagation within the vehicle for WPAN application.
- WP 6:** Verification of usability of the mmW, UWB, and optical bands for particular application and determination of accessible parameters.

1.2 SoMoPro Project

The SoMoPro project [2] is a three year (2014-2016) Marie Curie COFUND activity jointly funded by European Commission under the seventh framework program (FP7) and by the region of South Moravia, Czech Republic. The title of the project is, 'Localization using ultra wide band wireless systems: from algorithms to hardware implementation'.

Localization with current global positioning system (GPS) is restricted to the areas where there is a clear line-of-sight (LoS) to satellites. Apart from that, the resolution is very poor (within several meters) for local use. While indoor localization systems do exist (ultrasound, infrared etc.) they are expensive, hard to install and maintain, and suffer from similar resolution problems.

UWB nodes are relatively cheaper, transmit low power, and are capable of accurate localization in dense cluttered environments, owing to their inherent high delay resolution and ability to penetrate obstacles. Rather than competing GPS, UWB may augment the capabilities of GPS and operate in a compatible manner. UWB can provide detection, ranging, and motion sensing of personnel and objects through walls with centimeter precision.

The overall objective of the project is to examine UWB transmission as a possible candidate for localization purposes. In order to align the research with the GACR project activities, we have chosen the vehicular environment as our primary target application area.

1.3 Organization of the Chapter

After briefly reviewing the project objectives, we present the theoretical background of the three channel sounding architectures in Section 2. Section 3 deals with the measurement setup and parameters. The measurement setups and important results for experiments in UWB (3-11 GHz), mmW (55-65 GHz) and narrowband (5.8 GHz) are documented in Section 4, Section 5, and in Section 6, respectively. This chapter concludes with a description of future project activities in Section 7.

2 Channel Sounding Techniques

A basic wireless channel sounding experiment refers to exciting the channel with some known radio frequency (RF) signal and measuring the response (amplitude and phase) of the channel. As physical wireless channels can be approximated as linear filters, the impulse response of the channel completely characterizes the channel [3].

Depending on the frequency range of the sounding signal, radio channel sounding can be either narrowband or wideband. Further, the radio sounding can also be grouped under either time domain or frequency domain sounding. The impulse response, $h(t)$, obtained in Section 2.2 and Section 2.4 characterizes the channel in the time domain, while Section 2.3 characterizes the channel in the frequency domain by finding the channel transfer function, $H(f)$, approximated with the forward transmission coefficient, s_{21} . It is possible to convert one to another through Fourier transform [4]. As the measurements are all done with digital devices, the Fourier transforms employed are the fast Fourier transform (FFT) to get the transfer function from the CIR, $H(f) = \mathcal{F}\{h(t)\}$, and the inverse fast Fourier transform (IFFT) to obtain the CIR from s parameters, $h(t) = \mathcal{F}^{-1}\{H(f)\}$.

2.1 Channel Parameters

The field work related to our projects [1, 2] consists of various channel sounding experiments performed inside or around a passenger car parked in an underground garage. The static condition of the vehicle as well as fixed transmitter (Tx) and receiver (Rx) antenna positions allows us to neglect Doppler shift and time variations of the channel.

Channel impulse response: The baseband complex channel impulse response (CIR) under such assumptions may be expressed as follows

$$h(t) = \sum_{k=0}^N \alpha_k \exp(j\theta_k) \delta(t - \tau_k) \quad (1)$$

where the received signal is a composition of N multi-path components (MPCs), and α_k , θ_k and τ_k denote the path gain, phase shift and delay of the k th path, respectively. Unless used for localization purposes, the measured delay for the first arriving line of sight (LoS) path is set to zero, i.e. $\tau_0 = 0$, so that the delays for other non line of sight (nLoS) paths, i.e. $\tau_k; k \neq 0$, may be termed as excess delays.

Power delay profile: The power delay profile (PDP) is defined as the expectation of the average received power as a function of delay time when an impulse is transmitted. It is closely related with the CIR [5]

$$\text{PDP}(t) = \mathcal{E} \{ |h(t)|^2 \} \quad (2)$$

For comparison, the obtained PDPs are often described in the normalized form

$$\text{PDP}_n(t) = \text{PDP}(t) / \int_0^{\tau_{\max}} \text{PDP}(t) dt \quad (3)$$

where $\tau_{\max} = \max_k(\tau_k)$ denotes the maximum excess delay.

Mean excess delay: As the name implies, mean excess delay, denotes the weighted average delay and may be found from the first moment of the PDP

$$\bar{\tau} = \int_0^{\tau_{\max}} t \cdot \text{PDP}_n(t) dt \quad (4)$$

RMS delay spread: Root mean square (RMS) delay spread is the second central moment of the PDP

$$\tau_{\text{rms}} = \sqrt{\int_0^{\tau_{\max}} (t - \bar{\tau})^2 \cdot \text{PDP}_n(t) dt} \quad (5)$$

2.2 Direct Time Domain Sounding

If the channel is assumed to be linear and time invariant, the received signal, $r(t) = s(t) * h(t)$, may be expressed as the convolution of the transmitted signal $s(t)$ and the channel impulse response $h(t)$. Thus, the most straightforward way to find the channel impulse response is to send an impulse as the transmitted signal, $s(t) = \delta(t)$, which yields a CIR

at the receiver according to, $r(t) = \delta(t) * h(t) = h(t)$. However, the generation of an ideal impulse is not possible, and in practice an impulse like waveform with narrow pulse width is transmitted. It may be mentioned here that this method is primarily suitable for UWB measurements.

The main advantage of the pulsed sounding technique is, the channel impulse response is recorded in real time. In general, a repetitive pulse train is used for such sounding which necessitates fast acquisition at the receiver side. If a digital sampling oscilloscope (DSO) is used for this purpose, it should be able to operate at sampling rates of 20 Gs/s [6]. In our experiments we did not employ periodic pulse sounding as we did not try to observe the time variance of the channel.

There are several drawbacks associated with this method. First, the method needs special function generators. In fact, we abandoned this approach after first few set of experiments due to hardware unavailability. Second, impulsive signals are difficult to amplify due to RF amplifier nonlinearities [7]. Third, the poor dynamic range limits application of this method for larger Tx-Rx separations.

2.3 Frequency Domain Sounding

Frequency domain channel sounding is generally implemented through a vector network analyzer (VNA). The VNA uses a stepped frequency sweep to measure the channel in the frequency domain and records the forward transmission parameters. For a simple two port VNA this boils down to the recording of s_{21} , when the Tx and Rx are connected to port 1 and port 2, respectively.

The main benefits of the VNA are its large dynamic range, flexible frequency control, and smooth hardware synchronizations. Also the same setup may be used for both narrowband and wideband sounding by changing simple settings of the VNA. The requirement that Tx and Rx antennas should be within cable length and the channel to be static are also satisfied for in-car sounding experiments.

However, the VNA systems suffer from a slow measurement time [8]. One should also keep in mind that the CIR obtained with VNA through the IFFT operation is, $h_{\text{VNA}}(t) = h(t) * h_{\text{fil}}(t)$, where $H_{\text{fil}}(f) = \mathcal{F}\{h_{\text{fil}}(\tau)\}$ is the transfer function of the windowing operation.

2.4 PN Sequence based Time Domain Sounding

Pseudo noise (PN) sequence based time domain sounder use the following principle [4, 9]: if white noise, $n(t)$, is fed as input to the channel, and the received signal, $r(t) = \int h(\tau)n(t-\tau)d\tau$, is cross correlated with a delayed version of the input, the correlator output

$$\begin{aligned} \mathcal{E}\{r(t) \cdot n^*(t-\tau)\} &= \mathcal{E}\left\{\int h(\xi) \cdot n(t-\xi) \cdot n^*(t-\tau)d\xi\right\} \\ &= \int h(\xi) \cdot R_n(\tau-\xi)d\xi = N_0 \cdot h(\tau) \end{aligned} \quad (6)$$

is proportional to the impulse response of the channel. In the above set of equations, $R_n(\tau)$ is the autocorrelation function of white noise $n(t)$, which is equal to the single-

sided noise power spectral density, N_0 . A PN sequence is a long sequence having noise like properties.

In our experiment, we have used maximal length sequences or m -sequences as pseudo random binary sequences (PRBSs) due to their good autocorrelation properties. At the transmitter, a correlation sounder is thus composed of a PN sequence generator and at the receiver data may be recorded with a DSO. It is possible to realize a matched filter in the DSO matched to the specific m -sequence that was generated and obtain the impulse response in real time. We preferred to do the processing off-line with MATLAB after collecting the received signal samples from the DSO.

The PN sequence based method overcomes the low dynamic range problem of direct time domain sounding due to the inherent processing gain achieved by the cross correlation process. Correlation processing also suppresses narrowband interference signals. The post-processing is, however, a bit complex, and an accurate synchronization between Tx and Rx is needed [6].

3 Measurements Setup and Parameters

3.1 Measurement Parameters

There are some important measurement parameters, as listed below, which affects measurement accuracy and speed.

Frequency Range and Bandwidth: In VNA based measurements, the entire frequency range between a start frequency (f_L) and a stop frequency (f_H) is swept. The number of discrete frequency tones generated by the VNA (N_{VNA}) in the range and the bandwidth, $BW = f_H - f_L$, determine the frequency resolution

$$f_s = (f_H - f_L) / (N_{VNA} - 1) = BW / (N_{VNA} - 1) \quad (7)$$

On the other hand, the frequency response of an impulse like wave spans over from DC ($f_L = 0$) to a high cut-off frequency (f_H). The bandwidth, $BW = 2/t_d$, is determined by the duration of the pulse, t_d . For the PN sequence based setup, t_d should be replaced with T_c , the chip duration.

Time and Distance Resolution: For VNA, the bandwidth also determines the time resolution or the minimum time between samples in the CIR function obtained after IFFT

$$t_{res} = 1/BW \quad (8)$$

The distance resolution refers to the length an electromagnetic wave can propagate in free space ($c = 3 \times 10^8$ m/s) during time t_{res}

$$d_{res} = c \cdot t_{res} = c/BW \quad (9)$$

For direct time domain pulse sounding, the duration of the pulse (t_d) sets the time resolution, with minimum resolvable delay between MPCs being equal to pulse duration. If the pulse is narrower it is possible to resolve two close MPCs. Quite naturally, the chip duration (T_c) determines the time resolution for a PN sequence based setup.

Maximum CIR Length: The frequency step size (f_s) of the VNA determines the maximum observable delay spread, i.e. the maximum time delay until the MPCs are observed and the corresponding distance range [5] are

$$L_{\text{CIR}(t)} = 1/f_s \quad \text{and} \quad L_{\text{CIR}(d)} = c/f_s \quad (10)$$

On the other hand, if only a single pulse is transmitted, $L_{\text{CIR}(t)}$ is limited by the storage capacity of the receiver oscilloscope. For time domain periodic pulse sounding, the repetition rate determines the maximum unambiguous delay spread or impulse response length [9]. Thus

$$L_{\text{CIR}(t)} = N_{\text{PN}} \cdot T_c \quad \text{and} \quad L_{\text{CIR}(d)} = c \cdot N_{\text{PN}} \cdot T_c \quad (11)$$

are the maximum unambiguous range for PN sequence based setups. It may be noted that for m -sequences the length of PN sequence, $N_{\text{PN}} = 2^k - 1$, where k is a positive integer.

Dynamic Range: The dynamic range is defined by the difference between the largest and smallest amplitudes of the received multipath components

$$\text{DR} = 20 \log_{10} [\max\{h(t)\} / \min\{h(t)\}] \quad (12)$$

which can be directly evaluated from the CIR. The minimum amplitude of $h(t)$ refers to the value still observed above the noise floor. Alternately, a ratio between the peak amplitude and noise floor can be used to measure DR. This definition is generally used for VNA measurements.

For a PN sequence based sounder, the DR may be found from [10]

$$\text{DR} = 10 \log_{10}(N_{\text{PN}}) = 10 \log_{10}(2^k - 1) \quad (13)$$

This is also known as the processing gain (PG).

In frequency domain sounding, there are certain other parameters of interest such as intermediate frequency filter bandwidth (BW_{IF}) and output transmit power of the VNA (P_{VNA}). If P_{VNA} is set to 0 dBm, the s parameters correspond to the received power measured in dBm. Further, P_{VNA} and the noise floor together define the dynamic range. On the other hand, by reducing BW_{IF} the measurement accuracy can be improved. The cost paid is the increase in the measurement time.

3.2 Test Vehicle and Parking Lot Environment

The vehicle under study is a right-hand drive, regular four-door sedan Skoda Octavia III (model 1.8 TSI Combi) with dimensions 4.659m (length) \times 1.814m (width) \times 1.462m (height), which was parked six storeys beneath ground level in the multi-floored underground garage of the Faculty of Electrical Engineering (FEKT), Brno University of Technology (VUT). Reinforced concrete walls and floors of the garage provided us with an environment that was free from any narrowband interference (e.g. WiFi, Cellular). Also, there were no other cars parked in close vicinity [11].



Fig. 1. Underground garage where the measurements were conducted (left) and test vehicle (right).

3.3 Tx/Rx Antennas and their Placement

Vertically polarized monopole conical antennas were used for UWB sounding experiments. As suggested by Fig. 2, the radiation pattern exhibits omnidirectional characteristics over H-plane which is invariant in the frequency band of interest. Since the radiation pattern of the conical monopole antenna [12] is very close to the omnidirectional radiation pattern, we were able to capture a maximal number of multipath components (reflected waves). Due to a variable gain in the lower half E-plane radiation pattern (elevation angle from 90° to -90°), the antennas were placed in the car compartment so that the upper half E-plane radiation pattern, which is almost constant, was used. It means that when the antenna was placed at the cabin ceiling, it was set as bottom up. However, the reflected waves arriving from Tx antenna or incident on Rx antenna at lower elevation angles might be affected by the non-ideal radiation pattern of the antennas.

For the mmW band, we used a pair of open rectangular waveguide antennas (WR 15) for transmission and reception. As seen from Fig. 2, the radiation patterns are non-uniform. Currently, some work on developing slot antennas for mmW band are in

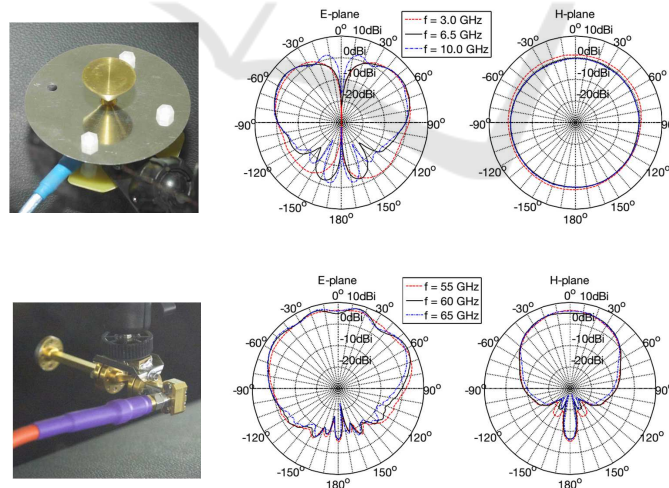


Fig. 2. Antenna used for UWB (top) and mmW (bottom) measurements with corresponding radiation patterns.

progress which would result in more uniform patterns [13]. For both UWB and mmW measurements, in order to avoid a degradation of the measured phase accuracy due to movements of the Rx antenna, phase-stable coaxial cables were used and included in the calibration process.

During the measurements, the Rx antenna had been placed on the driver's seat and on all other seats beside and behind the driver to imitate a hand-held mobile wireless device that belongs to either the driver or to a passenger. A plastic photographic tripod (JOBY GorillaPod) was used to maintain proper height (hand to lap separation) of the Rx antenna. The tripod was useful to keep the inverted cone base of the antenna in horizontal position for the UWB band and it helped in mounting the the Rx antenna in a face-to-face orientation for mmW band.

Determination of the Tx antenna positions were governed by two parallel objectives. First, the positions should resemble possible installation site for future in-vehicle wireless systems. For example, in modern cars the back roof may serve as a wireless docking station because this place usually contains some wiring and antenna for audio system or GPS. The second goal is to realize both LoS and nLoS scenarios.

4 Measurements in the Ultra Wide Band

The UWB measurements formed the majority of our activities as the the experiments overlaps with the activity plan for both the projects, GACR [1] and SoMoPro [2]. We have developed 3 different channel sounding set-ups using the available off-the-shelf hardware. The first set-up reflects a basic time-domain approach and involves pulse sounding. To improve the dynamic range, another time-domain set-up based on PN sequence was later developed. The third set-up pertains to frequency domain sounding and was realized using a VNA.

4.1 Direct Time Domain Measurements

The UWB time domain channel sounding measurements were performed inside the passenger compartment of the car in static condition. A Gaussian sine pulse was generated through the Tektronix AWG70002A waveform generator and was amplified through a high power amplifier (HPA) before feeding the signal to a wideband conical monopole antenna. The probing pulse used for intra vehicular UWB channel sounding has the form

$$s(t) = \sqrt{2\sqrt{2}/(t_d\sqrt{\pi})} \exp\left[-(t/t_d)^2\right] \cos(2\pi f_c t + \phi) \quad (14)$$

having unit energy, initial phase $\phi = 0.6\pi$, and an effective pulse duration of $2t_d = 0.276$ ns on either side. The carrier frequency, $f_c = 6.5$ GHz, was set at the middle of the FCC approved band (3GHz to 10GHz).

At the receiver side an identical conical monopole antenna is placed which receives the signal. The signal is then amplified through a low noise amplifier (LNA) and viewed/stored in a digital sampling oscilloscope Tektronix DPO72004C. For the HPA, we used Wenteq broadband power amplifier ABP1200-01-1825 which provided a gain of around 19 dB, whereas for the LNA, a Wenteq ABL1200-08-3220 was used that had a small

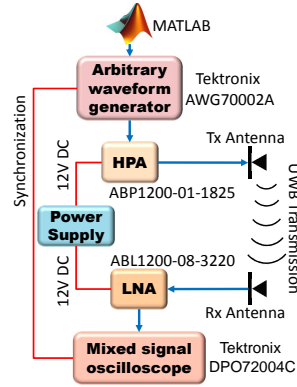


Fig. 3. UWB time domain measurement setup [14].

signal gain of 32 dB and a noise figure of 2 dB. Fig. 3 depicts the interconnections of the apparatus.



Fig. 4. Antenna placement in the car [14], RED: Tx antennas, BLUE: Rx antennas.

As shown in Fig. 4, a total of 52 different Tx-Rx antenna positions, with separations ranging from 0.56m to 1.9m, were tested with different degrees of passenger occupancy. Some measurements were repeated to investigate temporal variation, which were found to be negligible. It may be noted that although the car can accommodate four persons, we could vary the passenger count (including the driver) only up to three, as one of the places was always occupied by the receiver antenna and its attachments.

The received signal, $r(t)$, for a particular measurement can be represented as

$$r(t) = h_{Rx,Ant} * h(t) * h_{Tx,Ant} * s(t) = s_{ref}(t) * h(t) \quad (15)$$

where $h_{Tx,Ant}$ and $h_{Rx,Ant}$ are the impulse responses of the Tx and Rx antennas, and $s_{ref}(t) = h_{Rx,Ant} * h_{Tx,Ant} * s(t)$ is the reference input *template* that was obtained by measuring the response of the input $s(t)$ in an anechoic chamber free from reflectors/ diffrac-

tions. The reference distance between Tx and Rx antennas for measurement of $s_{ref}(t)$ was set to 1 m.

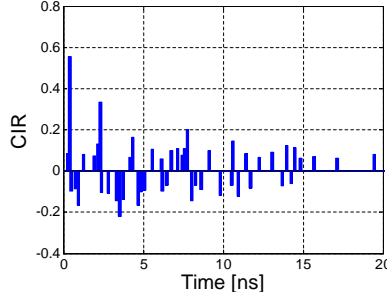


Fig. 5. Extracted CIR through modified CLEAN [14].

Next, CIRs were obtained by deconvolving the received signals with the input template using the modified CLEAN algorithm. The modified CLEAN algorithm [15] was faster and more accurate than the basic CLEAN algorithm [16] as shown in [14] through a detailed statistical performance comparison over a standard IEEE 802.15.3 channel simulation testbed. A typical impulse response is shown in Fig. 5 with the Tx antenna set at the left side of the windscreen near the roof (2L in Fig. 4) and the Rx antenna is placed on a tripod on the rear passenger seat on right (4R in Fig. 4) position. In general, it was found that nLoS conditions yielded more MPCs in the CIR compared to the cases when a direct LoS path exists between Tx and Rx antenna. This was due to presence of multiple reflected and diffracted paths inside the passenger compartment. The dynamic range can be increased by decreasing the threshold of the deconvolution algorithm. However, there is a possibility that fictitious entries would appear in the CIR profile due to noise, if the threshold is set too low.

Next, the CIR profiles obtained after the postprocessing via CLEAN were utilized to extract the RMS delay spread. After analyzing RMS delay spread values for different Tx-Rx distances, it was found that there exists only a weak correlation. On the other hand, it decreased consistently with higher passenger occupancy across all different Tx-Rx settings. For example, when the TX and Rx antennas were set to positions 4R and 1L positions (refer to Fig. 4), τ_{rms} values were 6.8880 ns, 6.3442 ns, 5.6712 ns and 4.9847 ns with no passenger, with driver (D), with driver and front passenger (D and FP) and with driver, front passenger, and the rear passenger on left (D, FP, and RPL), respectively. The reduction in delay spread can be accounted for the obstruction and absorption of several MPCs by human body.

4.2 Frequency Domain Measurements

The frequency domain measurements were realized with a 4 port vector network analyzer Agilent Technologies E5071Ca inside the passenger compartment of the car. Three ports were connected to three transmitting antennas and the fourth port was connected to a receiving antenna. The multiple input single output (MISO) channel sounding setup is shown in Fig. 6, and the measurement parameters are listed in Table 1. The

scattering parameters, i.e. s_{41} , s_{42} and s_{43} , were recorded which serve as the frequency domain channel transfer functions.

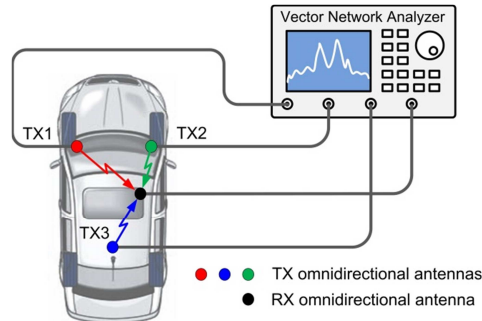


Fig. 6. UWB MISO measurement setup [17].

Table 1. VNA parameters for UWB measurement.

Parameter	Description	Value
f_L	Start frequency	3 GHz
f_H	Stop frequency	11 GHz
BW	Bandwidth	8 GHz
N_{VNA}	Number of points	801
f_s	Frequency step size	10 MHz
t_{res}	Time resolution	0.125 ns
d_{res}	Distance resolution	3.75 cm
$L_{CIR(t)}$	Maximum CIR length (time)	100 ns
$L_{CIR(d)}$	Maximum CIR length (distance)	30 m
BW_{IF}	IF filter bandwidth	100 Hz
P_{VNA}	Transmit power	5 dBm
$H_{fil}(f)$	Windowing for IFFT	Blackmann

The Rx antenna is placed at various locations inside the car compartment, on all seats and in the boot, and the Tx) antennas are placed on the left and right side of the dash-board, top corners of the windshield and at the rear part of the ceiling. There were altogether 90 possible Tx-Rx combinations (for details of antenna placement, please refer to [17]). The channel measurements are carried out for both, LoS and nLoS scenarios. nLoS is caused by the backrest of the seats, the dash-board, and/or persons sitting inside the vehicle.

When a statistical description of the received amplitude is attempted, it was found that they obey a generalized extreme value (GEV) process of type I

$$f(x) = (1/\sigma) \exp[-z - \exp(-z)] \quad ; \quad z = (x - \mu)/\sigma \quad (16)$$

with μ being the location parameter and σ the distribution scale parameter. Fig. 7 shows PDF of the received signal magnitudes in dBm fitted with the GEV statistics.

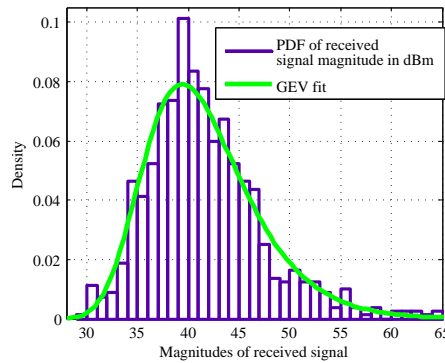


Fig. 7. Received signal amplitude statistics [17].

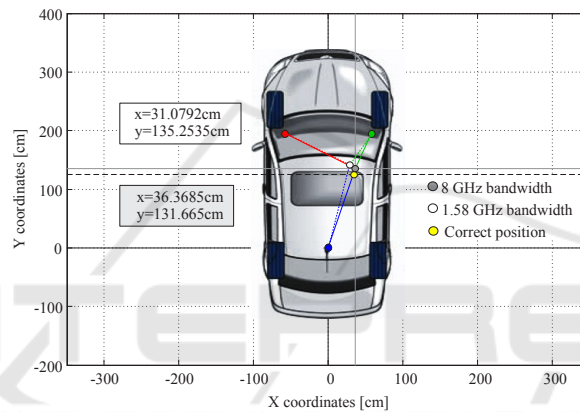


Fig. 8. Localization of the Rx antenna using TOA [17].

The experiment was repeated for a part of the whole UWB bandwidth, from 3.168 GHz to 4.752 GHz, with a bandwidth of 1.58 GHz as specified in the band 1 of the ECMA 368 standard [18], with 159 frequency points maintaining the same frequency step size (f_s). The goal was to test the feasibility of ranging and localization in the whole UWB and its part. The receiver antenna position was estimated through the time of arrival (TOA) technique, i.e. by finding rough distance of the Rx antenna from three Tx antennas and performing subsequent ranging in two dimension (2D).

The whole process involved four steps, namely calculation of the CIR, detection of the first incident ray, calculation of the Tx-Rx distances for all 3 Tx antennas, and finally performing the Rx antenna localization. The first ray arrival was detected through a peak search algorithm to find the strongest MPC above the noise floor. However, the drawback was, if the first or direct path is immersed in the noise floor, the algorithm fails. This situation is encountered in mostly nLoS cases where the direct path is highly attenuated. Once the first ray is detected, the corresponding distance is calculated by multiplying the delay (τ_0) with the traveling speed of electromagnetic wave (c). Finally, the RX antenna localization is achieved through the trilateration technique [18]. Using

the three calculated distances this technique allows 2D localization. Fig. 8 displays the result of localization in both the bands. The Rx antenna was placed on front passenger seat. It was important to identify the seat as in most in-vehicle localization applications (e.g. smart air bag, personalized communication profile etc.) we need to know the seat of the passenger holding the electronic communication device.

The error in ranging was less when the whole UWB was utilized rather than the first band. Also the ranging errors increased considerably in presence of passengers. The possible sources of error are, difference between calibration plane and phase center of antenna, inaccurate reference measurement, inaccuracy in estimating the first ray detection due to sampling, incorrect MPC detection and variation of wave propagation velocity in nLoS conditions [17].

Next, in another set of experiments, we used a similar 3×1 MISO setup and shifted the receiving antenna over a 10×10 spatial grid using a polystyrene rack having a 3 cm grid distance [19]. The idea was to study the spatial channel stationarity evaluated via Pearson correlation coefficients between absolute values of measured CIRs. The device configuration and the measurement parameters listed in Table 1 were unaltered except the frequency step size which was increased to 100 MHz for a faster measurement cycle. Further, the windowing for IFFT was rectangular in this set of experiments.

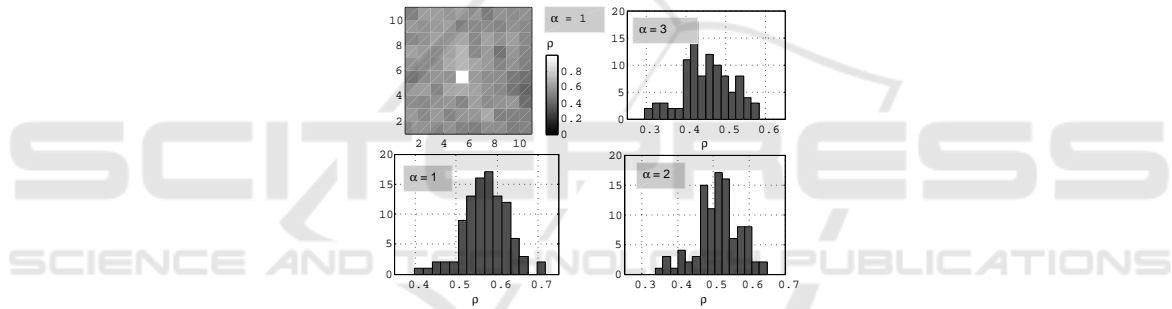


Fig. 9. Map of the correlation coefficient and their histograms [19].

Results of the spatial stationarity study are plotted in Fig. 9. The plots reflect the square geometry of our polystyrene rack. For Tx 1 ($\alpha = 1$), the map of correlation coefficient (ρ) shows that the impulse response in time domain is spatially stationary with a mean value of $\rho_1 \approx 0.55$. This behavior is typical also for Tx 2 ($\alpha = 2$) and Tx 3 ($\alpha = 3$). The histograms of ρ_1 , ρ_2 and ρ_3 are also plotted in Fig. 9.

The complex channel transfer functions ($H(f)$) obtained through the various set of measurements were converted to the respective envelope delay profiles or EDPs ($|h(t)|$) through IFFT operation. It was observed that the EDP is composed of large-scale variations (LSV), $\wp(t)$, and small-scale variations (SSV), $\xi(t)$. Further, the LSV part can be characterized by two different exponentially decaying functions, applicable to two different range of delay spreads

$$\wp(t) = \begin{cases} \wp^1(t) & ; 0 \geq t < \tau_b \\ \wp^2(t) & ; \tau_b \geq t < \tau_{\max} \end{cases} \quad (17)$$

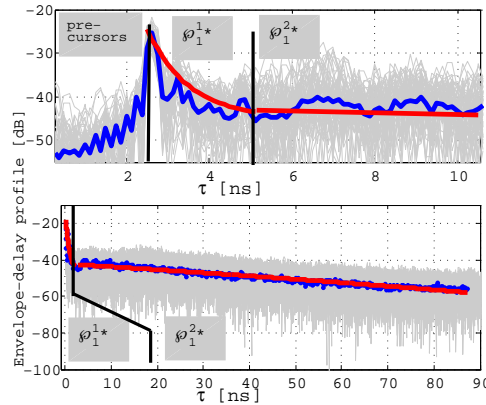


Fig. 10. Average EDP and the LSV parts [19].

where

$$\wp^1(t) = A + B \exp(-C \cdot t), \quad \wp^2(t) = D \exp(-E \cdot t), \quad (18)$$

and τ_b refers to the breakpoint in the delay spread domain. For our case it was about 4 ns. Fig. 10 shows the two different parts of the LSV of the PDP for the link between Tx 1 and Rx.

For the SSV, there exists no deterministic model as it is random. Exploiting the maximum likelihood estimation (MLE), we parametrized the superimposed SSV, $\xi(t) = \text{EDP}(t) - \wp(t)$, using the GEV distribution. The combined model of EDP was validated through a two-sample Kolmogorov-Smirnov (K-S) test.

4.3 PN Sequence based Time Domain Measurements

Compared to the direct time domain setup, a PN sequence based time domain sounder is simple to realize and replicate, provides correlation gain and does not sacrifice dynamic range much. It is also generally cheaper and faster than the VNA based frequency domain setup.

The time domain channel sounder utilizing pseudo random binary sequences (PRBS)

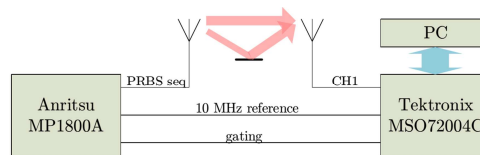


Fig. 11. PRBS based measurement setup [20].

for UWB was built from several off-the-shelf laboratory instruments as depicted in Fig. 11. The PRBS is generated via Anritsu signal quality analyzer MP1800A at a rate of $f_{\text{PN}} = 12.5$ Gbits/s with maximum RF output power of 13 dBm. At full rate the output

chip duration is $T_c = 1/f_{PN} = 80$ ps. Our m sequence used a k value of 11, which gives a processing gain, $PG = 10 \cdot \log_{10}(2^{31} - 1) \approx 31$ dB. There is no point in using a higher k value, i.e. lengthening the m sequence as the PDP will contain the same information with extended noise floor. Additional processing gain as well as dynamic range can be obtained by averaging the repeated trail of sequences. Also the value of T_c and k determine the maximum length of CIR in time and in distance domains, which according to (11) are, 163.76 ns and 49.13 m, respectively.

DSO Tektronix MSO72004C is utilized as a receiver. It provides 4 channels, 16 GHz bandwidth, 50 GS/s real time acquisition rate and 31.25 ms of data storage per channel which equals to 0.625 ms at sampling rate of 50 GS/s. As the acquisition rate of the DSO is 4 times of f_{PN} , the same chip is sampled 4 times. Another point to note is, for $k = 11$, the time period of the m sequence is, $T_p = N_{PN} \cdot T_c = 163.76$ ns, and only $N_{meas} = 0.625\text{ms}/163.76\text{ns} = 3816$ CIRs can be captured at once. Nevertheless, using advanced triggering modes, the number can be increased. It is also possible to continuously stream the real time acquired data to a personal computer (PC).

The signal quality analyzer also provides 10 MHz reference and gating or triggering signal to the oscilloscope. These are used for synchronization purposes. Compatible HPA and LNA may be included in the Tx and Rx chains, respectively, to boost the dynamic range of the system. A PC can be used to control the instruments and interchange data to provide additional features (e.g. real-time and continuous channel sounding) but is not necessary for the data acquisition.

The received data is correlated with the same transmitted PN sequence. For faster calculation, the correlation operation in the time domain is realized as a multiplication operation in the frequency domain. This action has some additional advantages too. For UWB, the band of interest is 3 GHz to 11 GHz. The spectral components outside this band is filtered out in the frequency domain.

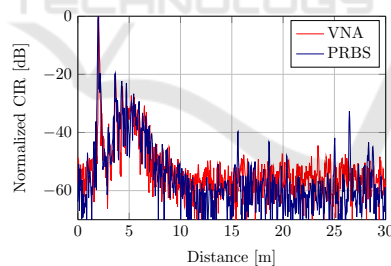


Fig. 12. Comparison of CIR measurements using VNA and PRBS based system [20].

In Fig. 12, a comparison of measurement results utilizing VNA and the proposed system is shown. The measurements were performed in an anechoic chamber with conical monopole antennas separated by 2 m distance from each other. Received time domain signal was amplified utilizing external LNA. The horizontal axis of Fig. 12 is expressed in spatial distance instead of time lag delay. It clearly shows the first arriving multipath component at time corresponding to the distance of 2 m. There are some other multipath components that start arriving at the distance 3.64 m, which is caused by re-

flections from laboratory instruments, antenna holders and feeding cables. This picture clearly shows the agreement between measurements performed by the VNA and proposed system. However, the measurement carried out by PRBS system contains some spurious peaks caused by non-linear devices in the measurement chain [21].

Recently, using this setup, UWB measurement in both the time and frequency domain for comparison purpose were also performed. The antenna positions for the both domain were set identical. Currently, the results are being analyzed.

5 Measurements in the mmW Band

For time domain measurement in the millimeter wave band, it was originally proposed to use a similar setup used in Section 4.1, i.e. with an arbitrary function generator and DSO, and the signal would be up converted to the mmW band before feeding it to a compatible Tx antenna (and down converted before feeding it to the DSO). An UWB to mmW FC1005V Silversima up-down converter was procured for the purpose. However, the large group delay (1ns/GHz) prohibited us using the setup. Thus the mmW band measurements performed so far are restricted to the frequency domain which are realized with a VNA.

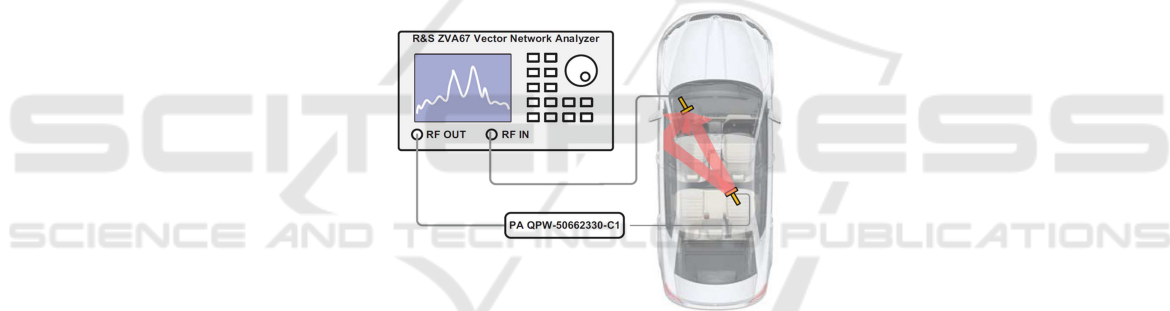


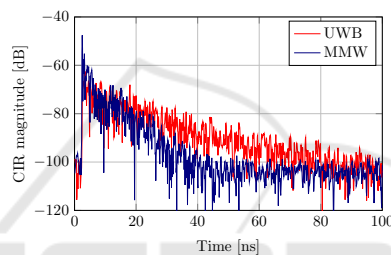
Fig. 13. mmW measurement setup [22].

In the first set of experiments, a 4-port vector network analyzer, Rhode and Schwarz ZVA67, was used for measuring the transmission coefficient between two mmW antennas in the frequency band 55-65 GHz. Because of the low output power available at analyzer transmitter output, Quinstar power amplifier QPW-50662330-C1 was utilized to raise the transmitted signal level, thus only one signal path (instead of three in the UWB band) could be measured at once. The single input single output (SISO) channel sounding setup is shown in Fig. 13, and other measurement parameters are listed in Table 2.

The places for Tx antennas are chosen to imitate handheld mobile devices that belong to a person sitting in the car. Furthermore, the Rx antennas are located to have a good coverage of vehicle space. A pair of open waveguide WR15 were used as Tx and Rx antennas. The measurement setup was calibrated for zero transmission while the waveguides were connected to each other.

Table 2. VNA parameters for mmW measurement.

Parameter	Description	Value
f_L	Start frequency	55 GHz
f_H	Stop frequency	65 GHz
BW	Bandwidth	10 GHz
N_{VNA}	Number of points	1001
f_s	Frequency step size	10 MHz
t_{res}	Time resolution	100 ps
d_{res}	Distance resolution	3 cm
$L_{CIR(t)}$	Maximum CIR length (time)	100 ns
$L_{CIR(d)}$	Maximum CIR length (distance)	30 m
BW_{IF}	IF filter bandwidth	100 Hz
P_{VNA}	Transmit power	5 dBm
$H_{fil}(f)$	Windowing for IFFT	Hanning

**Fig. 14.** Comparison of mmW CIR with UWB CIR [23].

A comparison of the CIRs obtained in the UWB and mmW band, when Tx antenna was at driver seat and Rx antenna is on the left side of the dashboard, is shown in Fig. 14. It can be seen that mmW CIR profile decays faster than the UWB. Moreover, the peak (caused by first/ direct path arrival) in mmW band is more distinctive compared to the UWB band peak. This is caused by frequency dependence of absorption parameters of materials that are used in modern cars [24].

Next, a comparison of ranging accuracies in the UWB and mmW band was attempted [25]. There were a series of steps involved in order to estimate the Tx-Rx distance. First, the measured complex channel transfer function was converted to the corresponding complex CIR function through IFFT. A Hann window was applied to mitigate leakage in time domain. Then, the first peak in absolute magnitude of CIR profile was detected utilizing semi-adaptive algorithm. The algorithm works with a threshold calculated from the maximum and mean value of the absolute magnitude of CIR, and it reports the first value above that threshold. A proper peak is identified in the neighborhood of that delay spread point. The distance corresponding to the detected peak is computed by multiplying the delay value and speed of light.

The ranging experiment in an empty car showed that while the distance measurement is having an average error and standard deviation of error of 6.7 cm and 8.3 cm for UWB, the values are 1.2 cm and 4.5 cm for the mmW band. For an occupied car, a

switch from UWB to mmW would cause to lower the average error from 9 cm to 2 cm and the standard deviation is reduced from 10.1 cm to 4.5 cm [23]. It may be concluded that mmW band is more suitable for precise distance measurement, probably due to favorable material properties, therefore enhancing the distinctiveness of the first arrival multipath component. However, one should keep in mind that during experiments, the antenna positions were not identical for UWB and mmW because of the physical dimensions of used antennas. The maximum difference is 29 cm, but it is less in most of the cases. Also the distance was measured manually with a ruler which might introduce some error in measurement.

In another set of experiments, we used same waveguides as antennas. The device configuration and the measurement parameters listed in Table 2 were unaltered except the windowing for IFFT which was rectangular in this set of experiments. The Rx antenna has been placed at different spatial points inside the car compartment, on all seats, trunk and in front of the seats. The Tx antenna has been placed on the left and right side of the dash-board and at the rear part of the ceiling (for details of antenna placement, please refer to [22]).

Based on the data obtained from the measurement we proposed a channel model for mmW band utilizing a similar approach as in [19], i.e. decomposition of the magnitude-delay profile into the small and large scale variations. The LSV trend has been found by the Hodrick-Prescott [26] detrending filter. A Hodrick-Prescott filter works like a moving average filter and it separates the trend and cyclical components but do not cause data loss. On the other hand, we found out that the best fit to the superimposed SSV is achieved by the GEV distribution.

There had been also subsequent mmW measurements in frequency domain using ZVA67, QPW-50662330-C1, and Rotagrip precision cross table (for antenna positioning). The aim of this measurement was to study the spatial stationarity in the mmW band. The spatial grid used for antenna positioning was set to 4 mm. The same mmW measurement with the Quinstar low noise preamplifier QLW-50754530-I2 and with application of the extended calibration technique using mmW attenuator in order to get larger SNR was also performed. The data set is currently being analyzed.

6 Narrowband Measurements

Due to large popularity of the Wireless Access for the Vehicular Environment (WAVE) technology in the 5.8 GHz band, we carried out a few measurements in this narrowband domain and compared our results with UWB.

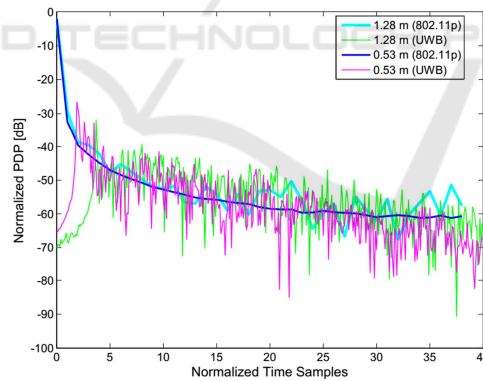
For measuring and recording the transmission coefficient between transmitter and receiver, a 4-port VNA from Agilent Technologies, E5071C [27] was used. The measurement parameters are listed in Table 3. A single input multiple output (SIMO) measurement setup was realized with one Tx and three Rx antennas. The four omni directional conical monopole antennas that were used are identical. Real and imaginary parts of the transmission coefficients (s_{x1}) were exported to MATLAB. The frequency domain data over the entire bandwidth $BW = 100$ MHz were partitioned into 10 MHz bins, where each bin corresponds to a sub-channel of 802.11p. All results were transformed from the frequency domain into the time domain utilizing the IFFT with a typ-

Table 3. VNA parameters for narrowband measurement.

Parameter	Description	Value
f_L	Start frequency	5.775 GHz
f_H	Stop frequency	5.875 GHz
BW	Bandwidth	100 MHz
N_{VNA}	Number of points	801
f_s	Frequency step size	0.125 MHz
t_{res}	Time resolution	10 ns
d_{res}	Distance resolution	3 m
$L_{CIR}(t)$	Maximum CIR length (time)	8 μ s
$L_{CIR}(d)$	Maximum CIR length (distance)	2.4 km
BW_{IF}	IF filter bandwidth	100 Hz
P_{VNA}	Transmit power	0 dBm
$H_{fil}(f)$	Windowing for IFFT	Rectangular

ical rectangular window. The PDP was calculated by averaging over 10 sub-channel time domain data.

A total of 15 different Tx-Rx combinations were tested with separations ranging from 0.53 m to 3.38 m. The Tx antenna was placed at three different locations inside the vehicle and at two locations outside the vehicle. In-car Tx antenna positions were set at the right rear seat, armrest in the middle of the car, driver seat, while for locations outside the car two positions at a height 1.09 meters were chosen; one in front of the car, and the other one near the right headlamp. The Rx antennas were installed on the left and right upper edges of the windshield and on the roof in the rear part of the vehicle. The positions of antennas were chosen for realizing both LoS and nLoS scenarios.

**Fig. 15.** Comparison of narrowband PDP with UWB PDP [28].

We compared our results for 802.11p protocol with measurements for UWB (3 GHz - 11GHz) performed using the same VNA based setup. The number of measured points were the same, however, due to the larger BW (8 GHz) and a frequency step size of $f_s = 100$ MHz, we have a smaller time range $t_d = 1/f_s = 10$ ns. Thus we cannot compare the PDPs in an one-to-one basis. For analyzing LSV models we use a scaled comparison

instead. Fig. 15 shows the UWB and the 802.11p normalized PDP vs normalized time samples. For UWB, it was found that the PDP constitutes one (or a few) major peaks followed by somewhat linear decreasing slope. The reader may also note the delay and lower power for the first peak of the UWB PDP. In addition, the delay and the maximum value of the peak is more for larger distances between the transmitting and receiving antennas. However, this phenomena is not observed in narrowband 5.8 GHz measurements for 802.11p.

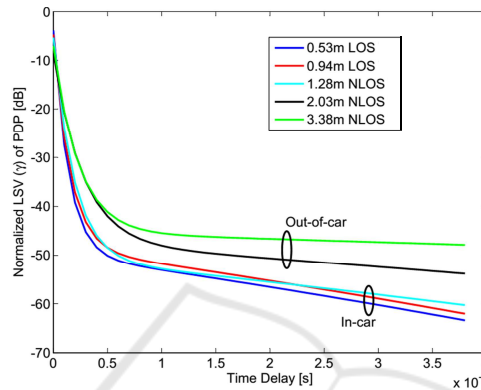


Fig. 16. The average trend of the PDP for narrowband measurements [28].

As far as the PDP is concerned, it includes LSV and SSV, which can be designated mathematically in the following manner: $PDP(t) = \wp(t) + \xi(t)$, where $\wp(t)$ denotes LSV and $\xi(t)$ is the SSV. We expressed the LSV with a two-term exponential model

$$\wp(t) = A \exp(B \cdot t) + C \exp(D \cdot t) \quad ; 0 < t < \tau_{\max} \quad (19)$$

where the first term includes power from direct and major reflected rays, and the second term, with a very low slope (close to linear) reflects the power from diffused multipath components. The LSVs for the two-term exponential model for different distance between Tx and Rx antennas of 0.53 m, 0.94 m, 1.28m, 2.03 m, and 3.38 m are shown in Fig. 16. Next, the SSVs are separated from the PDP by subtracting the LSV, and are characterized utilizing logistic, GEV, and normal distributions. Two sample K-S tests validated that the logistic distribution is optimal for in-car, whereas the GEV distribution serves better for out-of-car measurements.

7 Future Activities

7.1 Measurements in the IR Band

The IR channel models for the intra-vehicle environment have been published in only a handful of literature [29], and active research is going on this field worldwide. The GACR project goal was to test the viability of intra vehicular IR WPAN systems. The

first few testbeds for measurement were prepared in line with the UWB and mmW setups, i.e. for frequency domain characterizations a VNA based setup was proposed with optical transmitter (OTx) and optical receiver (ORx) directly coupled with VNA measuring the band between 1 to 5 GHz. In time domain, it was proposed to realize the same with a pulse generator and an oscilloscope.

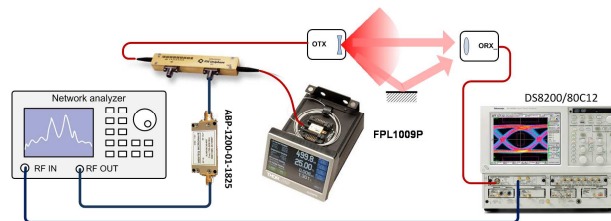


Fig. 17. IR measurement setup.

The IR measurement performed in time domain revealed some shortcomings of the IR measurement setup, e.g. limited modulation depth of the Mach-Zehnder modulator and large coupling losses between optical fibers and optical lenses resulting in very small SNR. For the new measurements the coupling losses were reduced by the modification and improvement of the mechanical parts of the OTx and ORx lenses leading to better focusing of the optical beams into the optical fibers. A planned measurement setup with network analyzer is shown in Fig. 17. The oscilloscope probe will be used as receiver. The optical signal will be generated from a Fabry-Perot FP 1009P laser and will be modulated by the RF signal, fed from analyzer through Wenteq ABP1200-01-1825 broadband power amplifier, with a JDSU APE microwave analog intensity modulator.

Analysis and modeling of the IR channel will be performed in the same way as in the case of UWB and mmW channel modeling. For the comparison purpose the same characteristics (PDP, excess delay and RMS delay spread, etc.) and statistics (data fitting by the proper distribution) will be studied and mathematical channel models will be created.

7.2 Localization

We will continue with the development of a robust algorithm for accurate estimation of the first multipath component arrival time (based on correlation receiver, matched filter receiver, receivers using various estimators such as maximum likelihood or mean square error estimator, or sparse signal reconstruction techniques). Then we are going to investigate the spatial distributions of the power path loss in the car compartment in order to analyze the accuracy of received signal strength (RSS)-based localization technique and its possible improvement using fingerprinting method. We would also like to assess possible application of the angle of arrival (AOA)-based positioning system and estimate its positioning capability. According to the topicality and desirability of the AOA-based positioning techniques we will measure the arrival angles and analyze

their statistical characteristics. All the above measurements will be performed for LoS and nLoS scenarios for an empty and an occupied car and for a different deployment of reference nodes.

7.3 Other Activities

In the next year, measurement in mmW band will be performed with the newly developed slot antenna array based on the substrate integrated waveguide (SIW) technology with significantly better omnidirectional radiation pattern compared to the formerly used open waveguide. Further we are going to examine effect of non-stationary environment in the car caused by running engine or loud sound produced by the built-in audio system or by the movement of passengers on the mmW channel characteristics. We also plan to extend the measurement to assess the effect and benefit of antenna arrays through the virtual array [30] approach and would perform some measurements in different brands of car and also in other vehicles such as tram or bus.

Acknowledgements. This work was supported by the SoMoPro II programme, Project No. 3SGA5720 *Localization via UWB*, co-financed by the People Programme (Marie Curie action) of the Seventh Framework Programme (FP7) of EU according to the REA Grant Agreement No. 291782 and by the South-Moravian Region. The research is further co-financed by the Czech Science Foundation, Project No. 13-38735S *Research into wireless channels for intra-vehicle communication and positioning*, and by Czech Ministry of Education in frame of National Sustainability Program under grant LO1401. For research, infrastructure of the SIX Center was used. The generous support from Skoda a.s. Mlada Boleslav are also gratefully acknowledged.

References

1. Department of Radio Electronics, Faculty of Electrical Engineering and Communication, Brno University of Technology: Research into wireless channels for intra-vehicle communication and positioning, No.: GACR-13-38735S. Project documentation page: <http://www.radio.feec.vutbr.cz/GACR-13-38735S/> (2013–16)
2. JCMM, South Moravian Programme for Distinguished Researchers (SoMoPro): Localization using ultra wide band wireless systems: from algorithms to hardware implementation, Call: SoMoPro-II-2012-IG, No.: 3SGA5720. Project documentation page: <http://www.jcmm.cz/en/aniruddha-chandra.html> (2014–16)
3. Molisch, A.F.: *Wireless Communications*. 2nd edn. John Wiley & Sons, West Sussex, England (2011)
4. Chen, Q.: *Wideband channel sounding techniques for dynamic spectrum access networks*. PhD Thesis, University of Kansas, Lawrence, KS, USA (2009)
5. Janssen, G.J.M., Stigter, P.A., Prasad, R.: *Wideband indoor channel measurements and BER analysis of frequency selective multipath channels at 2.4, 4.75, and 11.5 GHz*. *IEEE Trans. Commun.* 44 (1996) 1272–88
6. Pagani, P., Talom, F.T., Pajusco, P., Uguen, B.: *Ultra Wide Band Radio Propagation Channel*. John Wiley & Sons, New Jersey, USA (2013)
7. Costa, N., Haykin, S.: *Multiple-Input Multiple-Output Channel Models: Theory and Practice*. John Wiley & Sons, New Jersey, USA (2010)

8. Mao, X.H., Lee, Y.H., Ng, B.C.: Comparison of wideband channel sounding techniques. In: Proc. PIERS, Moscow, Russia (2009) 400–04
9. Parsons, J.D., Demery, D.A., Turkmani, A.M.D.: Sounding techniques for wideband mobile radio channels: a review. *IEE Proc. I (Communications, Speech and Vision)* 138 (1991) 437–46
10. Albornoz, J.M.: A wideband channel sounder. MS Thesis, Ohio State University, Columbus, OH, USA (2001)
11. Chandra, A., Blumenstein, J., Mikulasek, T., Vychodil, J., Marsalek, R., Prokes, A., Zemen, T., Mecklenbrauker, C.F.: Serial subtractive deconvolution algorithms for time-domain ultra wide band in-vehicle channel sounding. *IET Intell. Transp. Sys.* (2015) 1–11, In press
12. Kraus, J.D.: *Antennas*. Tata McGraw-Hill, New Delhi (1997)
13. Mikulasek, T., Lacik, J., Raida, Z.: SIW slot antennas utilized for 60-GHz channel characterization. *Microw. Opt. Technol. Lett.* 57 (2015) 1365–70
14. Chandra, A., Blumenstein, J., Mikulasek, T., Vychodil, J., Pospisil, M., Marsalek, R., Prokes, A., Zemen, T., Mecklenbrauker, C.: CLEAN algorithms for intra-vehicular time-domain UWB channel sounding. In: Proc. PECCS, Angers, France (2015) 224–29
15. Liu, T.C.K., Kim, D.I., Vaughan, R.G.: A high-resolution, multi-template deconvolution algorithm for time-domain UWB channel characterization. *Can. J. Elect. Comput. Eng.* 32 (2007) 207–13
16. Vaughan, R.G., Scott, N.L.: Super-resolution of pulsed multipath channels for delay spread characterization. *IEEE Trans. Commun.* 47 (1999) 343–47
17. Blumenstein, J., Prokes, A., Mikulasek, T., Marsalek, R., Zemen, T., Mecklenbrauker, C.: Measurements of ultra wide band in-vehicle channel - statistical description and TOA positioning feasibility study. *EURASIP J. Wirel. Commun. Net.* 2015 (2015) 1–9
18. Sahinoglu, Z., Gezici, S., Güvenc, I.: *Ultra-wideband Positioning Systems: Theoretical Limits, Ranging Algorithms, and Protocols*. Cambridge University Press, Cambridge, UK (2011)
19. Blumenstein, J., Mikulasek, T., Marsalek, R., Chandra, A., Prokes, A., Zemen, T., Mecklenbrauker, C.: In-vehicle UWB channel measurement, model and spatial stationarity. In: Proc. IEEE VNC, Paderborn, Germany (2014) 77–80
20. Vychodil, J., Chandra, A., Mikulasek, T., Prokes, A., Derbek, D.: UWB time domain channel sounder. In: Proc. MAREW, Pardubice, Czech Republic (2015) 1–4
21. Zetik, R., Kmec, M., Sachs, J., Thomä, R.S.: Real-time MIMO channel sounder for emulation of distributed ultrawideband systems. *Int. J. Ant. Prop.* 2014 (2014) 1–16
22. Blumenstein, J., Mikulasek, T., Marsalek, R., Prokes, A., Zemen, T., Mecklenbrauker, C.: In-vehicle mm-wave channel model and measurement. In: Proc. IEEE VTC, Vancouver, Canada (2014) 1–6
23. Vychodil, J., Blumenstein, J., Mikulasek, T., Prokes, A., Derbek, D.: Measurement of in-vehicle channel feasibility of ranging in UWB and MMW band. In: Proc. ICCVE, Vienna, Austria (2014) 1–4
24. Gustafson, C., Haneda, K., Wyne, S., Tufvesson, F.: On mm-wave multipath clustering and channel modeling. *IEEE Trans. Ant. Prop.* 62 (2014) 1445–55
25. Mecklenbrauker, C., Prokes, A., Blumenstein, J., Zemen, T.: Characterization of short range intra-vehicle wireless links comparing ultrawideband 3-11 GHz and millimeter waves 55-65 GHz. In: Proc. IEEE IMS, Phoenix, Arizona, USA (2015) 1–4
26. Hodrick, R.J., Prescott, E.C.: Postwar US business cycles: an empirical investigation. *Journal of Money, credit, and Banking* 29 (1997) 1–16
27. Muller, M.: WLAN 802.11p Measurements for Vehicle to Vehicle (V2V) DSRC. Application note Rohde & Schwarz: 1 MA152.Oe (2009)
28. Kukolev, P., Chandra, A., Mikulasek, T., Prokes, A., Zemen, T., Mecklenbrauker, C.: In-vehicle channel sounding in the 5.8 GHz band. *EURASIP J. Wirel. Commun. Net.* 2015 (2015) 1–9

29. Higgins, M.D., Green, R.J., Leeson, M.S.: Optical wireless for intravehicle communications: a channel viability analysis. *IEEE Trans. Veh. Tech.* 61 (2012) 123–29
30. Kolmonen, V.M.: Propagation channel measurement system development and channel characterization at 5.3 GHz. PhD Thesis, Aalto University School of Science and Technology, Espoo, Finland (2010)

